IEEE Access
Multidisciplinary | Rapid Review | Open Access Journal

IEEE POWER & ENERGY SOCIETY SECTION

Received September 8, 2020, accepted October 6, 2020, date of publication October 12, 2020, date of current version October 21, 2020.

Digital Object Identifier 10.1109/ACCESS.2020.3030160

Real-Time Implementation of Self-Adaptive Salp Swarm Optimization-Based Microgrid Droop Control

M. A. EBRAHIM[1], (Senior Member, IEEE), REHAM MOHAMED ABDEL FATTAH[2], EBTISAM MOSTAFA MOHAMED SAIED[1,3], SAMIR MOHAMED ABDEL MAKSOUD[1], AND HISHAM EL KHASHAB[2]

[1]Electrical Engineering Department, Faculty of Engineering at Shoubra, Benha University, Cairo 13518, Egypt
[2]Power Electronics and Energy Conversion Department, Electronics Research Institute, Cairo 12622, Egypt
[3]Electrical Engineering Department, High Technological Institute (HTI), 10th of Ramadan City, Egypt

Corresponding author: M. A. Ebrahim (mohamed.mohamed@feng.bu.edu.eg)

ABSTRACT This article presents a new version of the salp swarm inspired algorithm (SSIA) for the optimal design of the microgrid droop controller. The new version of SSIA is originated from the hybridizing of SSIA with the updating features of the particle swarm optimization (PSO). The development of SSIA is achieved by applying referential integrity between leaders and followers' candidates via employing both position and velocity update property of PSO. The hybrid SSIA-PSO also has a self-adaptive mechanism to avoid the necessity of refining the algorithm parameters for each optimization problem. Twenty-three benchmark test systems are tested to validate the superiority of the improved SSIA over the original PSO and SSIA. The proposed SSIA-PSO based control strategy is experimentally tested in a real-time environment. The control platform's performance is experimentally tested by using the Texas Instruments Launchpad TMS320F28379D. The developed real-time hardware-in-the-loop setup is a real investigation for implementing the suggested SSIA-PSO based control strategy with a low-cost control platform. The attained results prove the efficacy of the hybrid SSIA-PSO algorithm over the presented techniques. The introduced hybrid SSIA-PSO is employed to tackle the real microgrid droop control uncertainties such as inaccuracy in controller gains, deterioration of system parameters, multi-sources energy sharing challenge and system dynamics.

INDEX TERMS Droop control, microgrid, particle swarm optimization, salp swarm inspired algorithm, TMS320F28379D.

I. INTRODUCTION

Renewable energy resources (RERs) utilization becomes Required due to a moderate increase in electricity demand as well as pollution [1], [2]. Distributed generation sources (DGs), as a simple type of RERs, play a crucial role in keeping the continuity of supply for the end consumers, especially in the island mode of operation. DG units such as wind turbines (WTs), photovoltaic system (PVS), fuel cell (FC), and energy storage systems (ESSs) form microgrid, which must be operated in the grid-connected mode as well as island mode contingency [3]. Therefore, controlling frequency and voltage can be achieved using droop control on VSIs, especially in the isolated operation mode [4]. In the previous literature, droop controllers had been employed for sharing the powers of DG units [5], [6]. However, this approach has a major limitation in attaining optimal parameters or even the right results. With the advent of new optimization algorithms for solving many optimizations and engineering problems, the question still open "is there only optimization technique capable of solving all problems?" [7]. Recently, many optimization algorithms such as salp swarm inspired algorithm (SSIA) [8], moth-flame optimization techniques [9], sine cosine algorithm (SCA) [10], ant lion optimizer (ALO) [11], grey wolf optimizer (GWO) [12] and dragonfly algorithm (DA) [13] have been used to reach the

The associate editor coordinating the review of this manuscript and approving it for publication was S. Srivastava.

optimal solution with sufficient convergence performance. So, the hybrid theory can be used as a possible solution for achieving that harmony. In the last decade, various hybrid optimization techniques were provided for solving many engineering problems [14]. Kaur and Mahajan have built up a hybrid technique between the ant colony algorithm (ACA) and the particle swarm optimization (PSO) algorithm [15]. Touqeer *et al.* used the grasshopper optimization algorithm (GOA) on the islanded microgrid to find the gains of the PI controller [16]. Fatih and Asım *et al.* developed a hybrid technique between PSO and GWO algorithm [17]. Mehrdad Ahmadi applied the PSO on an islanded microgrid to calculate the gains of the PI controller [18]. The vision of this article is to present an improved version of SSIA based on the referential integrity property between SSIA and PSO compared to seven previously published metaheuristic algorithms. The attained findings of the comparative analysis consistently show that SSIA-PSO is highly competitive and can be used for various engineering and other issues. Moreover, the application of a hybrid SSIA-PSO algorithm to real engineering problem namely the microgrid droop control problem. Therefore, a microgrid test system consists of two sources and each source consists of a solar PV array, battery station (BS), supercapacitor (SC) is used to accomplish this study. Multiple performance aspects, including power-sharing process, frequency and voltage constrained limits during solar radiation, temperature and load changes, are evaluated to verify the effectiveness of the proposed hybrid SSIA-PSO comprehensively. In order to accelerate the suggested control strategy, prototyping, hardware-in-the-loop (HIL) is employed. In the last decades, HIL has been used intensively in many industries such as aerospace, automotive and testing distributed control systems, where the plants are especially complex [19]. In such systems, different loading conditions in the simulation model are simple to produce and thus the controller hardware can be checked in all required circumstances, some of which may even be dangerous in the real system. The HIL methodology can be expected to significantly speed up testing of control systems with reduced cost to test, reduce risks associated with failure as well as testing many plant variations while avoiding testing fault modes [20]. In this article, real-time test bed is developed based on typical HIL, all the suggested controllers are implemented on LAUNCHXL-F28379D while the remaining components of the system (PV, BS, SC) are simulated on the host PC. The LAUNCHXL-F28379D is type of digital signal processors (DSP). In the last decade, the architecture of DSP applications has been enhanced considerably. The DSPs are a major and important technology as they are focused on effective and more reliable checking for the functionality of the control system for large scale systems such as renewable energy systems[21]. The proposed control system is implemented using TI launchpad TMS320F28379D.

The major contributions of the article can be summarized as follow:

1) In this article, a new variant of the Salp Swarm Inspired Algorithm (SSIA) is developed by applying referential hybridization with Particle Swarm Optimization (PSO).
2) A solid comparative study is conducted to prove the capability of the suggested modified SSIA with seven different types of metaheuristic optimization techniques, including single as well as hybrid algorithm between Grey Wolf Optimizer and PSO
3) The developed hybrid SSIA-PSO had been suggested to solve one of the most popular microgrid technical problems presented in the optimal design for the parameters of PI controller and parameters of droop control to preserve fair power-sharing between different sources.
4) A real-time test bench is constructed using LAUNCHXL-F28379D to verify the theoretical findings of the suggested optimization technique. Moreover, a comprehensive comparative study is performed between the simulation and experimental results to demonstrate the efficacy of the proposed SSIA-PSO.

II. OPTIMIZATION METHODS

The proposed hybrid SSIA-PSO technique is a renowned method that originated from the hybridizing of SSIA with the updating features of PSO. The improvement of SSIA is achieved by applying referential integrity between leaders and followers' candidates via employing both position and velocity update property of PSO.

A. THE PARTICLE SWARM OPTIMIZATION

The idea of the PSO was inspired by the behavior of natural creatures such as fish schooling and birds flocking [22], [23]. The PSO mathematical equations can be represented by (1)-(3):

$$v_i^{k+1} = \beta(t) * v_i^k + d_1 r_1 \left(p_i^k - x_i^k\right) + d_2 r_2 \left(g_{best} - x_i^k\right) \quad (1)$$

$$x_i^{k+1} = x_i^k + v_i^{k+1} \quad (2)$$

$$\beta(t) = \beta_{max} - ((\beta_{max} - \beta_{min}) * 1/\max\_iter) \quad (3)$$

where

i: particle index k: number of iterations
v_i^k : velocity of particle i at iteration k
x_i^k : position of particle i at iteration k
β : inertia constant and it is often in the range [0 1]
d_1 and d_2: coefficients which are usually between [0 2]
r_1 and r_2: random values which are generated for each velocity update
p_i^k: local best position
g_{best} : global best position

The advantages of PSO are the capability to change the position of particles in a multi-dimensional search space. On the other side, the most important disadvantage of the PSO is that the regulation speed and direction of the particle are not exact. This method cannot be applied to the non-coordinate system, such as the energy field [24]. Therefore, the trend

towards hybridizing with another technique to get its advantages and avoid its disadvantages is crucial.

B. SALP SWARM INSPIRED ALGORITHM

Mirjalili *et al.* presented a new swarm intelligence method known as SSIA inspired by the behavior of salps [8]. The salp chains consist of two groups: leaders and followers. From the nature of salp's behavior, it can be observed that the leader salp moves around the food source and the follower salps follow the leader.

To update the position of the leader, the following equation is proposed [8], [25], [26]:

$$x_j^1 = \begin{cases} F_j + c_1\left(\left(ub_j - lb_j\right)c_2 + lb_j\right) c_3 \geq 0 \\ F_j - c_1\left(\left(ub_j - lb_j\right)c_2 + lb_j\right) c_3 < 0 \end{cases} \quad (4)$$

where

x_j^1 : first Salp (leader) position in the j^{th} dimension,
Fj: food source position of the j^{th} dimension,
ub_j: upper bound of j^{th} dimension,
lb_j: lower bound of j^{th} dimension,
l: current iteration
L: maximum number of iterations
c_1, c_2, and c_3: random
numbers uniformly generated in the interval of [0,1].
x_j^i : position of nth follower salp in ith dimension
c_1 is a significant coefficient which balances exploration and exploitation. The following equation is used to estimate c_1 [8], [25]:

$$c_1 = 2e^{-\left(\frac{4l}{L}\right)^2} \quad (5)$$

The position of the followers will be updated depending on Newton's law of motion as:

$$x_j^i = \frac{1}{2}ct^2 + \lambda_0 t \quad (6)$$

where I $\geq$2 and x_j^i shows the position of i^{th} follower salp in j^{th} dimension, t is time, λ_0 is the initial speed, and c = $\frac{\lambda_{final}}{\lambda_0}$ where $\lambda = \frac{x - x_0}{t}$.

For streamlining, it can be presumed that t is the iteration in an optimization problem; this equation can be expressed as follows:

$$x_j^i = \frac{1}{2}(x_j^i + x_j^{i-1}) \quad (7)$$

The advantages of SSIA are summarized in its high performance, implementation simplicity, low parameters and low cost of the account [8],[25]. Whereas the disadvantages originate from its possibility to be trapped into local minima, premature convergence, and slow searching. As a result, there is a tendency to use hybridization techniques to overcome the demerits of SSIA.

C. HYBRID SALP SWARM INSPIRED ALGORITHM AND PARTICLE SWARM OPTIMIZATION

There are many studies in which the hybrid process has been applied to many forms of heuristics by researchers. In this article, hybridizing PSO with SSIA is presented. The PSO has a good exploration property for the solution space with limited exploitation for the search agents. On the other hand, the SSIA has a competitive exploration of the solution space. The hybrid SSIA-PSO improves the facility of exploitation in PSO with the ability of exploration in SSIA. The compromising of both exploration and exploitation properties enhanced the capability of convergence to the optimal solution with shorter time and low computation burden. The pseudo-code of the SSIA-PSO algorithm is illustrated in Fig. 1. In equation (11), c_2 is modified from the existing one in the original SSIA version. In equation (12), the inertia constant β in conjunction with the velocity equation of PSO is employed to modify the leader x_j^1 position in SSIA, according to (13) and (14).

Initialize the salp population x_i (i = 1, 2, ..., n) considering u_b and l_b
PSO inertia constant β calculated by Eq. (3)
while (end condition is not satisfied)
Calculate the fitness of each search agent(salp)
F=the best search agent
SSIA c_1 calculated by Eq. (5)
modify c_2 by Eq. (11)
for each salp (x_i)
if(i==1)
SSIA the position of the leading salp calculation by Eq. (12)
PSO the velocity calculated by Eq. (13)
modify the position of the leading salp by Eq. (14)
else
PSO the velocity calculated by Eq. (15)
Modify the follower salp position x_j^i *and* x_j^{i-1} by Eq. (16) &Eq. (17)
Modify the position of the follower salp by Eq. (18)
end
end
Amend the salps based on the upper and lower bounds of variables
end
return F

FIGURE 1. The pseudo-code of the SSIA-PSO algorithm.

The modified mathematical model for calculating the position of the leader is presented as:

$$A = rand() \quad (8)$$

$$B = rand() \quad (9)$$

$$c_3 = rand() \quad (10)$$

$$c_2 = B - ((A - B)/\max\_iter) \quad (11)$$

$$x_j^1 = \begin{cases} \beta(t) * F_j + c_1\left(\left(ub_j - lb_j\right)c_2 + lb_j\right) & c_3 \geq 0 \\ \beta(t) * F_j - c_1\left(\left(ub_j - lb_j\right)c_2 + lb_j\right) & c_3 < 0 \end{cases} \quad (12)$$

$$v_j^{i+1} = \beta(t) * v_j^i + c_2 r_1\left(x_j^1 - F_j\right) \quad (13)$$

$$x_j^1 = x_j^1 + v_j^{i+1} \quad (14)$$

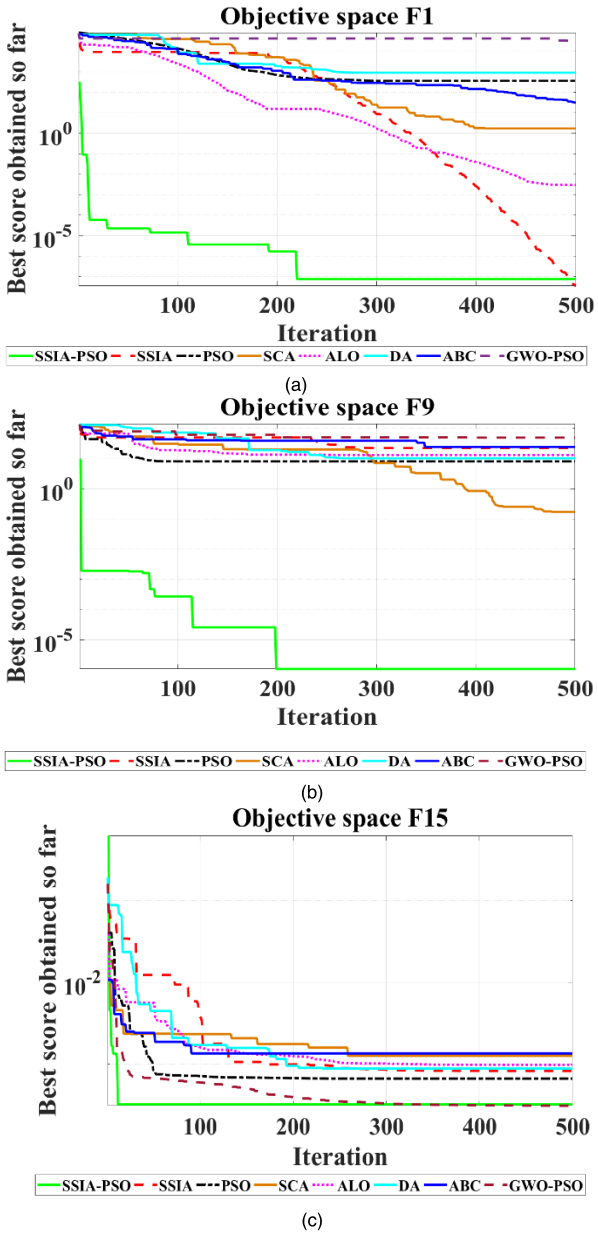

FIGURE 2. Convergence characteristics of SSIA-PSO, SSIA, PSO, SCA, ALO, DA, ABC and GWO-PSO: (a) Convergence characteristic to function F1, (b) Convergence characteristic to function F9, (c) Convergence characteristic to function F15.

The velocity equation of PSO, including inertia constant β is employed to modify the follower salp x_j^i and x_j^{i-1} position as derived in (15) – (18). Finally, the follower's positions of the hybrid SSIA-PSO technique can be determined according to (18).

$$v_j^{i+1} = \beta(t) * v_j^i + c_2 r_1 \left(x_j^i - x_j^1\right) \tag{15}$$

$$x_j^i = \beta(t) * x_j^i + v_j^{i+1} \tag{16}$$

$$x_j^{i-1} = \beta(t) * x_j^{i-1} + v_j^{i+1} \tag{17}$$

$$x_j^i = \frac{1}{2}(x_j^i + x_j^{i-1}) \tag{18}$$

The benefits of the hybrid are to combine the positive features of both PSO and SSIA to find the optimum global efficiency to tackle complex optimization problems such as the optimal operation of the microgrid.

D. TESTING FUNCTIONS AND RESULTS

The hybrid SSIA-PSO algorithm is applied to twenty-three-benchmark functions in this segment. The benchmark problems are consisting of three groups: unimodal, multimodal and fixed dimension multimodal functions. The convergence curves are the most common results in single-objective optimization literature. Moreover, the mean and standard deviation values can be used as performance indicators (PIs) for the enhanced behavior of SSIA-PSO compared to the other alternative metaheuristics. The attained results and convergence performance indicate that the SSIA-PSO is more reliable. Fig. 2 shows sample results for the convergence characteristics of SSIA-PSO, SSIA, PSO, SCA, ALO, DA, ABC and GWO-PSO during application to F1, F9 and F15. Table 1 presents the estimation for the standard deviation and mean values.

E. ANALYSIS AND DISCUSSION OF THE RESULTS

The maximum number of iterations is set to 500 and the number of search agents is 30. The capability test for the SSIA-PSO, SSIA, PSO, SCA, ALO, DA, ABC and GWO-PSO have activated 30 runs per function. Fig. 2 depicts a comparative study for the convergence performance of SSIA-PSO, SSIA, PSO, SCA, ALO, DA ABC and GWO-PSO. The SSIA-PSO shows its superiority in most benchmark functions over the alternative methods. The results obtained from the convergence performance showed that the proposed SSIA-PSO is more reliable. Table 1 reports the average and standard deviation of the attained statistical results over 30 runs. Table 1 proves that SSIA-PSO has the best result in F1, F2, F3, F4, F5, F7, F9, F10, F11, F13 and F15. Based on previous results, SSIA-PSO has the best performance due to combining advantages of both SSIA and PSO.

III. DROOP CONTROL STRATEGY OF MICROGRID

In the conventional power system, the turbine governor (TG) and the automatic voltage regulator (AVR) are employed to maintain the voltage as well as the frequency within limits. Unfortunately, both TG and AVR is not suitable for PVS and FC. For these reasons, the tendency to search for another alternative solution becomes mandatory. Thanks to droop control that can help in keeping the voltage and frequency during any change in load. Fig. 3 shows the topology of the microgrid control strategy, including three layers with their components that present a computational complexity issue for the controllers' designers and control practitioners. The three control layers with their computational complexity will be discussed in detail in the following subsections.

TABLE 1. Standard deviation and mean values for various metaheuristics during application to benchmark functions.

Test Functions		SSIA-PSO	SSIA	PSO	SCA	ALO	DA	ABC	GWO-PSO
F1	Average	3.19×10^{-23}	1.54×10^{-07}	1.30×10^{04}	2.69×10^{-12}	1.08×10^{-8}	5.22×10^{0}	2.38×10^{-05}	1.29×10^{03}
	Std	7.66×10^{-23}	1.48×10^{-07}	2.020×10^{-04}	7.91×10^{-12}	9.01×10^{-09}	9.10×10^{0}	2.26×10^{-05}	5.12×10^{03}
F2	Average	7.03×10^{-12}	4.00×10^{-04}	2.16×10^{-01}	9.26×10^{-10}	1.76×10^{0}	1.66×10^{0}	6.26×10^{-06}	9.76×10^{04}
	Std	2.62×10^{-11}	2.00×10^{-03}	4.490×10^{-01}	2.51×10^{-09}	6.99×10^{0}	1.14×10^{0}	5.22×10^{-06}	4.90×10^{05}
F3	Average	1.15×10^{-20}	5.38×10^{-07}	2.140×10^{03}	5.49×10^{-01}	3.21×10^{-02}	1.72×10^{02}	2.15×10^{02}	9.88×10^{03}
	Std	4.84×10^{-20}	1.11×10^{-06}	3.130×10^{03}	3.00×10^{0}	7.42×10^{-02}	1.72×10^{02}	1.02×10^{02}	1.91×10^{04}
F4	Average	1.32×10^{-12}	2.86×10^{-05}	1.25×10^{01}	1.05×10^{-03}	2.68×10^{-02}	3.49×10^{0}	3.72×10^{0}	1.66×10^{01}
	Std	2.02×10^{-12}	4.39×10^{-05}	1.72×10^{01}	2.58×10^{-03}	9.64×10^{-02}	3.05×10^{0}	7.79×10^{-01}	2.26×10^{01}
F5	Average	8.88×10^{0}	1.54×10^{02}	2.52×10^{02}	7.36×10^{0}	1.84×10^{02}	2.21×10^{03}	2.01×10^{01}	7.14×10^{06}
	Std	1.40×10^{-02}	3.13×10^{02}	5.39×10^{02}	3.81×10^{-01}	4.11×10^{02}	6.06×10^{03}	$2.1.8 \times 10^{01}$	2.52×10^{07}
F6	Average	6.97×10^{-01}	1.02×10^{-09}	9.27×10^{02}	4.52×10^{-01}	8.58×10^{-09}	6.78×10^{0}	3.06×10^{-05}	2.56×10^{03}
	Std	1.99×10^{-01}	3.69×10^{-10}	2.94×10^{03}	1.55×10^{-01}	4.17×10^{-09}	1.05×10^{01}	3.54×10^{-05}	7.56×10^{03}
F7	Average	1.32×10^{-04}	1.50×10^{-02}	1.30×10^{-02}	2.53×10^{-03}	2.60×10^{-02}	3.35×10^{-02}	1.38×10^{-02}	2.34×10^{0}
	Std	1.00×10^{-04}	9.00×10^{-03}	1.60×10^{-02}	1.97×10^{-03}	1.29×10^{-02}	2.19×10^{-02}	5.2×10^{-03}	6.77×10^{0}
F8	Average	-2.66×10^{03}	-2.72×10^{03}	-1.48×10^{03}	-2.11×10^{03}	-2.36×10^{03}	-2.76×10^{03}	-2.75×10^{03}	-7.38×10^{03}
	Std	4.03×10^{02}	2.70×10^{02}	2.69×10^{02}	1.98×10^{02}	5.87×10^{02}	3.07×10^{02}	3.00×10^{02}	9.19×10^{02}
F9	Average	0	1.75×10^{01}	1.12×10^{01}	2.17×10^{0}	2.15×10^{01}	2.94×10^{01}	2.89×10^{01}	7.18×10^{01}
	Std	0	7.44×10^{0}	7.04×10^{0}	5.81×10^{0}	9.78×10^{0}	1.09×10^{01}	5.51×10^{0}	6.67×10^{01}
F10	Average	1.23×10^{-12}	6.39×10^{-01}	3.12×10^{0}	1.92×10^{-07}	1.93×10^{-01}	2.80×10^{0}	3.36×10^{-02}	4.58×10^{0}
	Std	2.05×10^{-12}	9.88×10^{-01}	2.22×10^{0}	3.33×10^{-07}	4.38×10^{-01}	1.03×10^{0}	2.20×10^{-02}	5.65×10^{0}
F11	Average	0	2.60×10^{-01}	6.29×10^{01}	1.41×10^{-01}	2.27×10^{-01}	5.43×10^{-01}	4.18×10^{-01}	4.63×10^{01}
	Std	0	2.05×10^{-02}	4.90×10^{01}	2.38×10^{-01}	7.27×10^{-02}	2.85×10^{-01}	1.08×10^{-01}	9.57×10^{01}
F12	Average	1.36×10^{-01}	7.53×10^{-01}	5.72×10^{05}	8.97×10^{-02}	3.13×10^{0}	2.05×10^{0}	3.25×10^{-03}	1.08×10^{07}
	Std	5.60×10^{-02}	1.11×10^{0}	2.18×10^{06}	3.47×10^{-02}	3.35×10^{0}	2.05×10^{0}	1.29×10^{-02}	3.59×10^{07}
F13	Average	5.78×10^{-03}	1.10×10^{-03}	3.39×10^{06}	3.36×10^{-01}	1.43×10^{-03}	9.92×10^{-01}	8.91×10^{-03}	1.29×10^{07}
	Std	3.60×10^{-03}	3.30×10^{-03}	1.86×10^{07}	9.49×10^{-02}	4.63×10^{-03}	8.44×10^{-01}	5.36×10^{-03}	5.35×10^{07}
F14	Average	1.79×10^{0}	1.13×10^{0}	2.99×10^{0}	1.86×10^{0}	2.81×10^{0}	1.43×10^{0}	9.98×10^{-01}	4.09×10^{0}
	Std	1.06×10^{0}	3.43×10^{-01}	4.39×10^{0}	9.99×10^{-01}	2.04×10^{0}	8.89×10^{-01}	3.03×10^{-03}	4.16×10^{0}
F15	Average	3.37×10^{-04}	1.50×10^{-03}	2.00×10^{-03}	1.11×10^{-03}	2.17×10^{-03}	3.43×10^{-03}	1.16×10^{-03}	6.79×10^{-03}
	Std	1.94×10^{-05}	4.00×10^{-03}	3.70×10^{-03}	3.35×10^{-04}	4.95×10^{-03}	5.88×10^{-03}	1.23×10^{-04}	8.81×10^{-03}
F16	Average	-1.02×10^{0}	-1.03×10^{0}	-1.03×10^{0}	-1.03×10^{0}	-1.032×10^{0}	-1.03×10^{0}	-1.031×10^{0}	-1.032×10^{0}
	Std	4.50×10^{-03}	2.33×10^{-14}	7.61×10^{-07}	4.46×10^{-05}	9.41×10^{-14}	6.46×10^{-07}	9.27×10^{-08}	1.21×10^{-04}
F17	Average	3.98×10^{-01}	3.97×10^{-01}	3.98×10^{-01}	3.99×10^{-1}	3.979×10^{-1}	3.98×10^{-01}	3.979×10^{-01}	3.98×10^{-01}
	Std	3.70×10^{-04}	5.31×10^{-14}	2.28×10^{-04}	1.93×10^{-03}	1.58×10^{-13}	5.74×10^{-07}	2.82×10^{-05}	$2.91 \times 10^{0-06}$
F18	Average	3.29×10^{0}	3.00×10^{0}	3.00×10^{0}	3.00×10^{0}	3.00×10^{0}	3.00×10^{0}	3×10^{0}	3.00×10^{0}
	Std	3.72×10^{-01}	3.18×10^{-13}	5.21×10^{-05}	1.16×10^{-04}	5.69×10^{-13}	4.65×10^{-06}	4.95×10^{-06}	2.97×10^{-03}
F19	Average	-3.85×10^{0}	-3.86×10^{0}	-3.86×10^{0}	-3.85×10^{0}	-3.87×10^{0}	-3.86×10^{0}	-3.86×10^{0}	-3.86×10^{0}
	Std	1.10×10^{-02}	1.32×10^{-10}	3.10×10^{-03}	3.33×10^{-03}	2.14×10^{-13}	4.70×10^{-04}	4.05×10^{-10}	3.64×10^{-03}
F20	Average	-3.20×10^{0}	-3.23×10^{0}	-3.28×10^{0}	-2.83×10^{0}	-3.29×10^{0}	-3.24×10^{0}	-3.32×10^{0}	-3.14×10^{0}
	Std	7.40×10^{-02}	6.20×10^{-02}	6.40×10^{-02}	3.84×10^{-01}	5.56×10^{-02}	8.34×10^{-02}	4.28×10^{-06}	2.43×10^{-01}
F21	Average	-5.02×10^{0}	-3.23×10^{0}	-5.63×10^{0}	-2.38×10^{0}	-5.54×10^{0}	-7.37×10^{0}	-9.92×10^{0}	-6.96×10^{0}
	Std	1.10×10^{-02}	2.98×10^{0}	3.18×10^{0}	1.86×10^{0}	2.79×10^{0}	2.91×10^{0}	7.63×10^{-01}	3.55×10^{0}
F22	Average	-5.05×10^{0}	-8.85×10^{0}	-5.51×10^{0}	-3.49×10^{0}	-7.03×10^{0}	-7.05×10^{0}	-1.04×10^{01}	-7.78×10^{0}
	Std	1.50×10^{-02}	2.91×10^{0}	3.61×10^{0}	2.08×10^{0}	3.33×10^{0}	2.80×10^{0}	1.12×10^{-07}	3.35×10^{0}
F23	Average	-5.26×10^{0}	-8.66×10^{0}	-6.71×10^{0}	-4.27×10^{0}	-6.28×10^{0}	-8.14×10^{0}	-1.05×10^{01}	-8.07×10^{0}
	Std	9.164×10^{-01}	3.23×10^{0}	3.70×10^{0}	2.29×10^{0}	3.42×10^{0}	3.25×10^{0}	2.33×10^{0}	3.49×10^{0}

A. POWER CIRCUIT

The power circuit includes four parts as follows: the three-phase VSI, the resistive-inductive-capacitive (RLC) filter, the coupling inductor (L_2), and the three-phase load.

B. DROOP CONTROL

Droop control is a control approach usually applied to generators to allow parallel generator operation in the microgrid. It is based on the coupling between active power and frequency and reactive power and voltage [1], [27].

To calculate the active power (p) and the reactive power (q) before filter using output voltage (V_0) and output current (I_0), the V_0 and I_0 are transformed to dq reference frame for the calculation of (p) and (q) using (19) and (20) [2]:

$$p = V_{0d} I_{0d} + V_{0q} I_{0q} \tag{19}$$

$$q = V_{0d} I_{0q} + V_{0q} I_{0d} \tag{20}$$

For improvement, the p and q will pass in a low pass filter and will be renamed as P and Q. The P and Q are calculated according to (21) and (22), respectively:

$$P = \frac{\omega_c}{S + \omega_c} (v_{0d} I_{0d} + v_{0q} I_{0q}) \tag{21}$$

$$Q = \frac{\omega_c}{S + \omega_c} (v_{0d} I_{0q} + v_{0q} I_{0d}) \tag{22}$$

After calculating P and Q, the reference angular frequency ω and the reference voltage V will be calculated through (23)

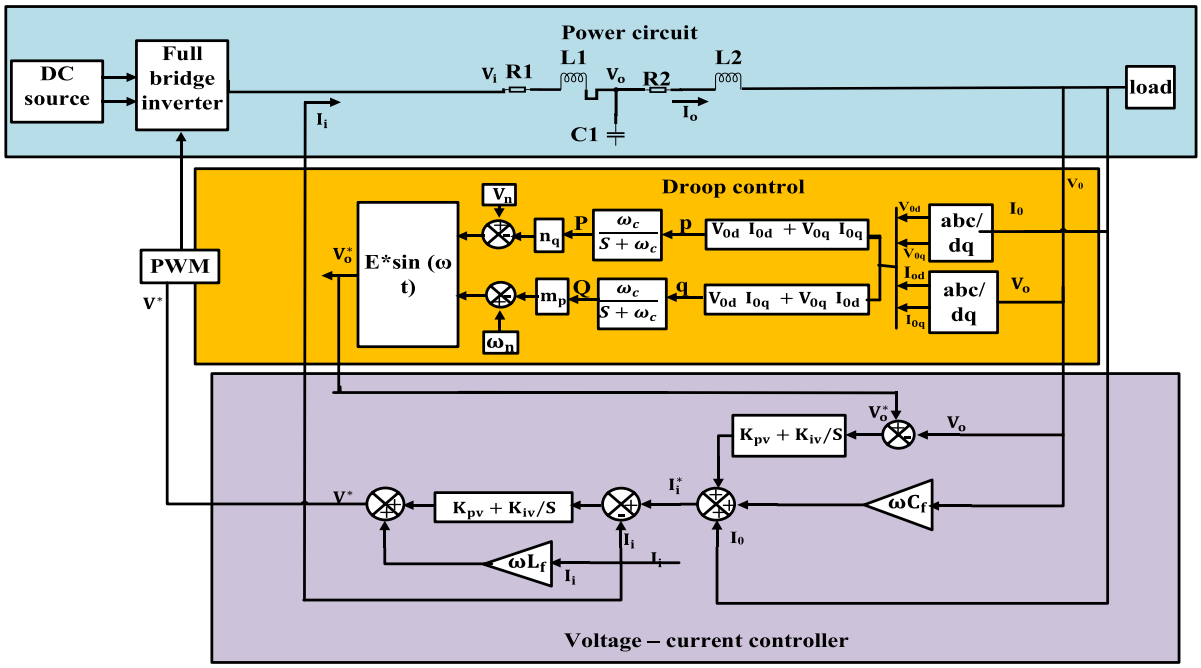

FIGURE 3. The system block diagram.

and (24):

$$\omega = \omega_n - m_p * P \tag{23}$$

$$V = V_n - n_q * Q \tag{24}$$

where ω_n and V_n are the constant coefficients of frequency and voltage characteristics, respectively and m_p, n_q are the coefficients of static droop.

C. VOLTAGE-CURRENT CONTROLLER

The reference voltage and frequency will be the input to the voltage controller to find the reference current (I_i^*). The voltage controller output I_i^* will be fed to the current controller. The current controller output (V^*) feds the pulse width modulation (PWM). The output of PWM is used to control VSI. To calculate I_i^* and V^*, equations (25) and (26) are employed [2].

$$I_i^* = -\omega C_f V_o^* + k_{pv}\left(V_o^* - V_o\right) + \frac{K_{iv}}{s}\left(V_o^* - V_o\right) \tag{25}$$

$$V^* = -\omega L_f I_i + k_{pc}\left(I_i^* - I_i\right) + \frac{k_{ic}}{S}\left(I_i^* - I_i\right) \tag{26}$$

where L_f is the coupling inductor

ω is the cut-off frequency

S is the Laplace transform parameter

The voltage and current are controlled by using the PI controller. The gains of the PI controller must be calculated exactly. There are many methods used to calculate gains of PI, such as the trial and error approach and root locus method. However, these methods cannot deal with the complex nonlinear system like microgrid or even determine exact controller gains. Consequently, the calculation of PI gains is very important, so this article will try to find the optimal gains of the PI controller by applying the new proposed algorithm SSIA-PSO.

IV. SSIA-PSO APPLICATION IN MICROGRID

The proposed SSIA-PSO technology has proven a success as an optimization tool, so it will be used to determine the optimal control parameters and coefficients of the droop control when there is a variation in the load. The control parameters and coefficients of the droop control (K_{p1}, K_{i1}, K_{p2}, K_{i2}, K_{p3}, K_{i3}, K_{p4}, K_{i4}, n_q, m_p) are obtained by SSIA-PSO to realize a minimized voltage and frequency fluctuations. Fig. 4 demonstrates the flowchart for the application steps of the proposed SSIA-PSO for tuning droop control parameters in the microgrid. Any optimization technique needs an objective function to perform its assigned task. This objective function is used to minimize the error between the measured and desired values. The four types of error benchmark objective functions are integral of absolute error (IAE), integral of square error (ISE), integral of time absolute error (ITAE), integral of time square error (ITSE)[28].

In this case study, the multi-objective function is employed to consider both the frequency and voltage errors via the accumulative sum property. Fig. 5 presents a diagram of the test system that consists of two solar PV array systems (SPVAS), DC-DC boost converter, two battery stations (BSs), supercapacitor (SC), three-phase VSI, load, and transmission line. The test system mimics the real microgrid considering the effects of the transient behaviors on the entire network. The load is shared equally as it is noticed from the autonomy of MG provided in Fig. 5. Two SPVAS are used. Moreover,

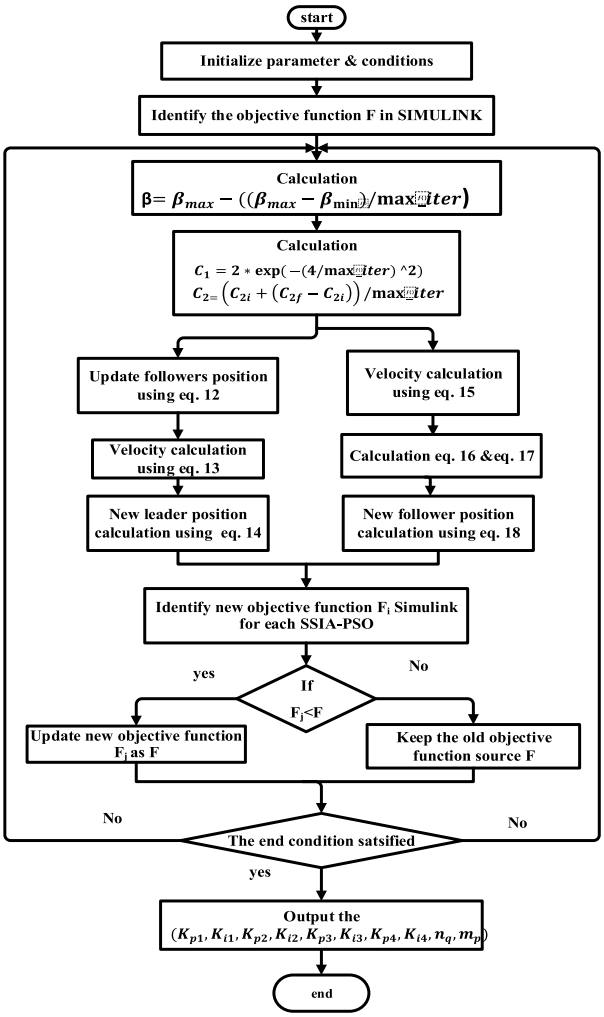

FIGURE 4. The flowchart of SSIA-PSO for droop control in microgrid.

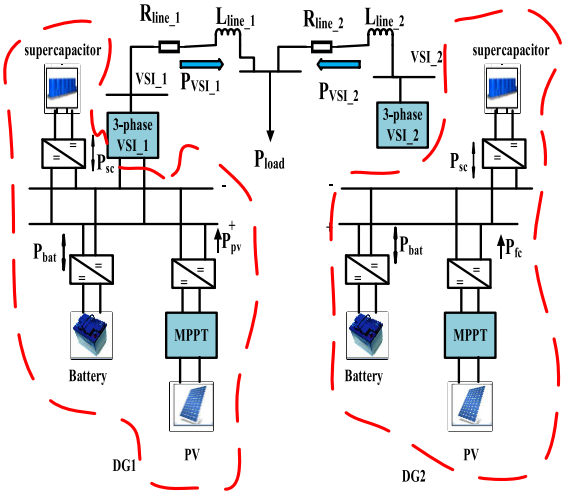

FIGURE 5. Test system diagram.

two battery stations are employed to assist the microgrid power quality. Also, supercapacitors are used to enhance the dynamic response of the microgrid due to their fast charging and discharging characteristics. The DC-DC boost converter is equipped with incremental conductance (INC) based maximum power point tracking control to extract the maximum power from the sun.

TABLE 2. Test system parameters [2].

Parameter	Value	Parameter	Value
V_{base}	380 V	ω_n	1 p.u.
S_{base}	100 kVA	V_n	1 p.u.
ω_{base}	314 red/sec	R_{line1}	0.14 p.u.
L_f	0.95 x10^{-3} p.u.	L_{line1}	2.1 x10^{-3} p.u.
C_f	35 x10^{-6} p.u.	R_{line2}	0.2 p.u.
R_f	0.067 p.u.	L_{line2}	3.5 x10^{-3} p.u.
L_c	0.23 x10^{-3} p.u.	P_{load}	70 x10^3
R_c	0.02 p.u.	ω_c	0.1 p.u.
Ts	5.144 x10^{-6} sec	Frequency of PWM	10 kHz
Power of PV	109.88 kW	Capacitance of supercapacitor	29 F
Power of battery	56kW		

TABLE 3. Gains of PI and droop control coefficients.

	IAE	ISE	ITAE	ITSE
Objective function	1.02 x10^7	4.86 x10^8	6.08 x10^6	3.52 x10^8
K_{p1}	0.729378	0.297968	0.312331	0.435606
K_{i1}	375.0570	584.8307	353.2782	492.2117
K_{p2}	0.608674	0.698931	0.550147	0.265350
K_{i2}	263.1959	559.3624	351.9411	284.2597
K_{p3}	8.185111	14.82072	15.30740	12.32775
K_{i3}	7580.512	14793.52	12837.96	10874.02
K_{p4}	12.03902	11.76199	8.163614	11.41256
K_{i4}	5232.952	8675.729	10772.97	14010.86
n_q	0.239131	0.374225	0.347973	0.345697
m_p	0.019751	0.013487	0.013713	0.020106
Time Taken (min)	199.8119	203.2725	205.7367	203.4736

The parameters of the test system (islanded microgrid model) are summarized in Table 2 [2]. The SSIA-PSO for droop control on microgrid is coded using Matlab™/Simulink environment (Release: 2019a). Simulations are carried on an Intel®core™ i5-8250u CPU. QM Process (1.60 GHz, 12.00 GB RAM) hp ProBook 4540s laptop.

To select the best type of objective function, the SSIA-PSO is applied to the test system for testing the four types of objective function.

Table 3 shows the various objective functions and values of K_{p1}, K_{i1}, K_{p2}, K_{i2}, K_{p3}, K_{i3}, K_{p4}, K_{i4}, n_q, m_p for each type using an SSIA-PSO optimization technique. The minimum objective function between the four types of error has been chosen. As a result, the ITAE has been chosen to run the microgrid system.

The comprehensive comparative study for the seven optimization techniques is provided in Table 4. The results confirm that SSIA-PSO succeeded in achieving the assigned control task with minimum voltage and frequency errors. For a fair comparison, seven alternative optimization tools (SSIA, PSO, SCA, ALO, DA, ABC and GWO-PSO) are employed to check the quality of SSIA-PSO.

TABLE 4. Results of the applied seven optimization techniques.

	SSA	PSO	SCA	ALO	DA	ABC	GWO-PSO	SSIA-PSO
Objective function	10.25 x10^6	12.66 x10^6	13.76 x10^6	11.22 x10^6	11.25 x10^6	18.460 x10^6	9.3545 x10^6	6.08 x10^6
K_{p1}	0.691433	0.557908	0.622222	0.532215	0.253903	0.641502	0.688742	0.312331
K_{i1}	311.4964	475.0824	242.9766	521.9489	382.4229	530.0400	537.406	353.2782
K_{p2}	0.548548	0.513765	0.288695	0.537495	0.386742	0.470766	0.381130	0.550147
K_{i2}	543.6527	565.1678	550.6742	537.8442	438.6973	349.2290	449.9315	351.9411
K_{p3}	11.27808	13.09909	7.515493	14.58615	9.276742	12.22560	15.16175	15.30740
K_{i3}	13879.68	12410.52	14587.14	6500.108	14416.69	6358.140	12187.15	12837.96
K_{p4}	10.25541	13.05646	6.854758	7.378885	8.530060	9.003440	14.31799	8.163614
K_{i4}	14414.39	11132.63	13968.29	10557.64	6300.102	13267.80	5846.391	10772.97
n_q	0.272247	0.225909	0.228627	0.367958	0.390588	0.266158	0.203386	0.347973
m_p	0.014868	0.009724	0.012441	0.014005	0.015810	0.015636	0.013584	0.013713
Time Taken (min)	207.2686	219.1358	218.7167	212.2842	209.5110	224.4803	207.5955	205.7367

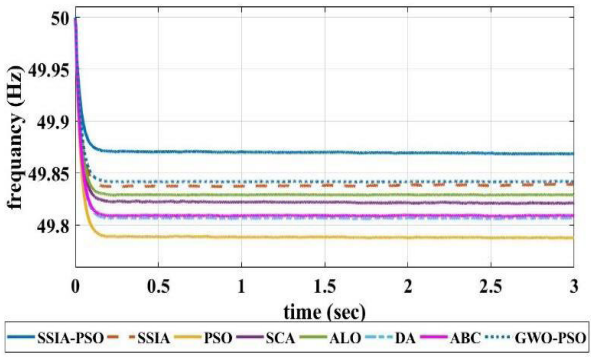

FIGURE 6. Frequency response of MG equipped with droop controller tuned via seven optimization techniques.

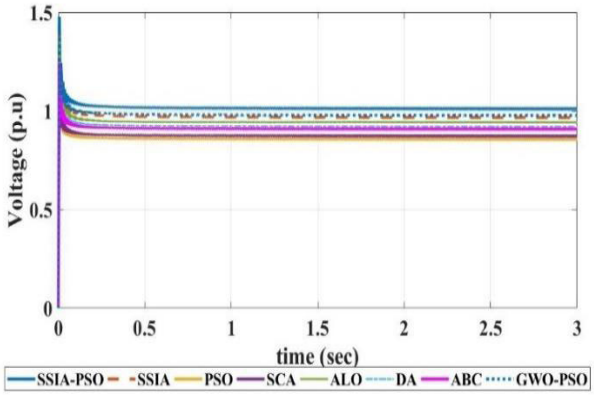

FIGURE 7. Voltage response of MG equipped with droop controller tuned via seven optimization techniques.

Fig. 6 shows the frequency response for MG equipped with droop controllers tuned using the seven suggested optimization techniques. As it is evident from the frequency response that SSIA-PSO supersedes the alternative meta-heuristics. In comparison, PSO alone has the worst frequency response. Fig. 7 demonstrates the effectiveness of SSIA-PSO in achieving good voltage behavior comparing to the other seven types of optimization.

V. SIMULATION RESULTS

The well-tuned controllers via hybrid SSIA-PSO are equipped on a microgrid test system to confirm the power-sharing between multi-sources as well as controlling the voltage and frequency. The two types of load: continuous change and ramp loads, are considered in this study with RERs variability, such as (variable irradiance and temperature).

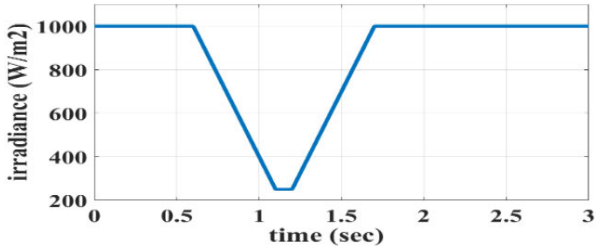

FIGURE 8. Solar irradiance variation pattern for all applied scenarios.

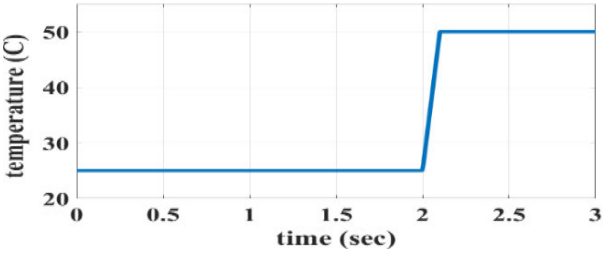

FIGURE 9. Solar temperature variation for all applied scenarios.

A. ISLANDING MODE WITH CONTINUOUS CYCLIC LOAD VARIATIONS SCENARIO (IMCCLVS)

The microgrid is worked in islanding mode under RERs variability with continuous cyclic load variations as 70 kW (0.7 p.u.) from 0-0.3 sec, and then the load value increased to 110 kW (1.1 p.u.) at 0.3- 0.7 sec; finally, the load value backs to 70 kW (0.7 p.u.) at 0.7- 1.2 sec at the end of the load cycle. Fig. 8 shows the ramp-up / down solar irradiance from 1000 W/m^2 to 250.

W/m^2. Fig. 9 demonstrates the temperature variation between 25 °C and 50 °C. Fig. 10 shows that each DG injects an equal amount of active power into MG. Noticeably, the rate of change in power is almost the same as the rate of change in load, which confirms the good tracking behavior for SSIA-PSO based droop controllers during IMCCLVS

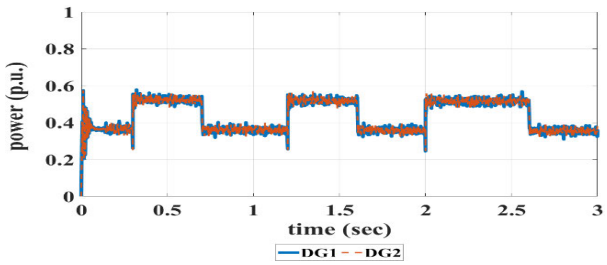

FIGURE 10. Active powers generated by DGs in IMCCLVS scenario.

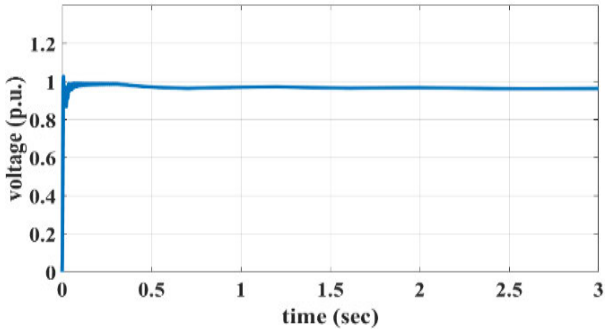

FIGURE 11. Voltage magnitude IMCCLVS scenario.

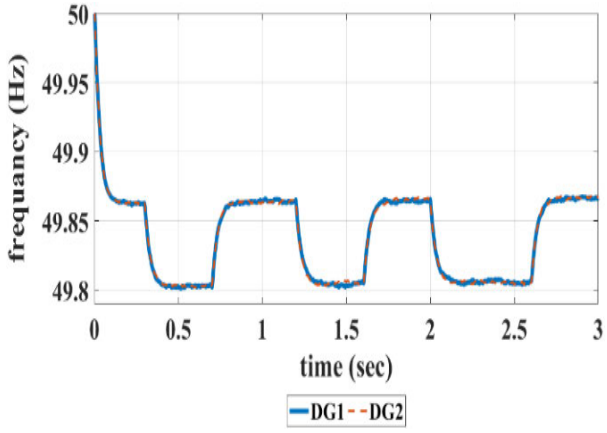

FIGURE 12. Inverter frequency of IMCCLVS scenario.

scenario. Fig. 11 and 12 indicate the voltage and frequency transient response during IMCCLVS scenario, respectively. Remarkably, Fig. 11 and 12 illustrate that the frequency response is strongly affected by the rate of change in power, while the voltage is slightly affected. Fig. 13 provides an insight view of how SSIA-PSO based droop control strategy presents a multi-sources energy management scheme. Moreover, Fig. 13 demonstrates how SPVASs, BSs, and SC interact with each other in dynamism to maintain the continuity of supply.

B. ISLANDING MODE WITH RAMP LOAD VARIATIONS SCENARIO (IMRLVS)

This scenario is like IMCCLVS scenario, but the ramp load variations are considered. The load value of 70 kW (0.7 p.u.)

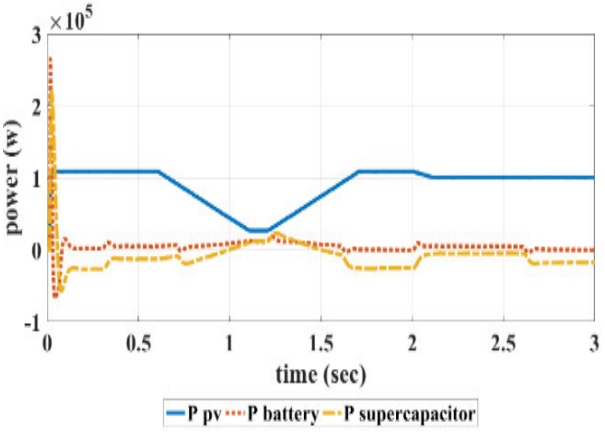

FIGURE 13. Powers of SPVASs, BSs, and SC in IMCCLVS scenario.

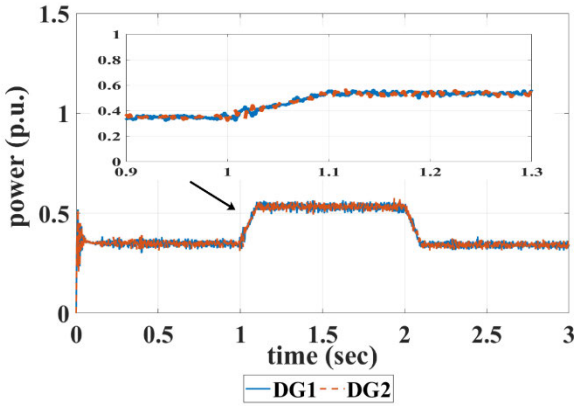

FIGURE 14. Active powers generated by two DGs IMRLVS scenario.

from 0- 1 sec, then increased to 110 kW (1.1 p.u.) at 1.1 sec, then backs to 70 kW (1.1 p.u.) at 2 sec. IMRLVS scenario presents the ramp load variation pattern, which is very close to the real operating conditions. Fig. 14 shows that active power is almost identical to each DG and shows that power increases or decreases gradually in the same way as the ramp load. It is worth mentioning that the proposed SSIA-PSO based droop controllers tracked the load power changes effectively with a good dynamic response. Moreover, the voltage and frequency in DGs during the load changes are maintained within the permissible limits, as shown in Fig. 15 and 16, respectively. Fig. 17 shows that both BSs and SC are collaborating to handle the period when SPVASs output power decreases due to RERs variability and the load is increased at the same time. Again, the continuity of supply is preserved due to the effective SSIA-PSO based droop control scheme.

VI. EXPERIMENTAL SETUP AND RESULTS

The hardware-in-the-loop provides real-time system verification between the simulation of the system under study and hardware testing for the suggested control strategy. The HIL approach requires host and target cooperation. One of the most important conditions that must be met for the

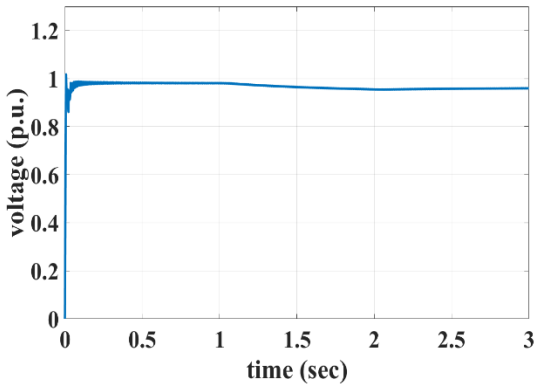

FIGURE 15. Voltage magnitude IMRLVS scenario.

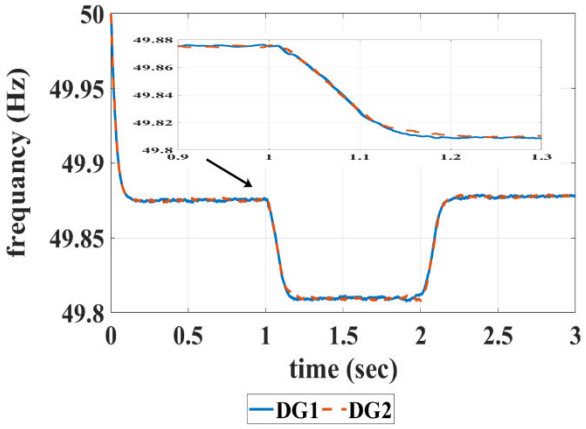

FIGURE 16. Inverter frequency of IMRLVS scenario.

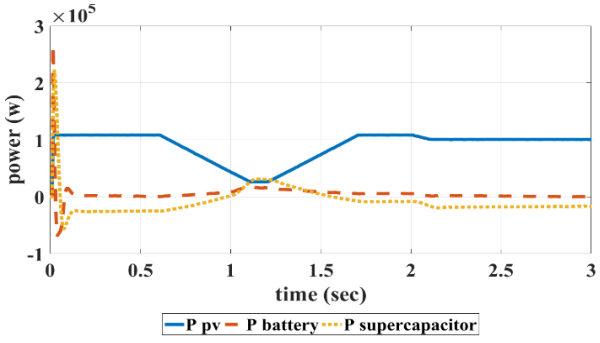

FIGURE 17. Powers of SPVASs, BSs, and SC in IMRLVS scenario.

application is that a communication link must be established between the host development platform and the target publishing platform [29]. To set up a simulation of the Hardware-in-the-loop, the connection to the Host PC-Target is configured. After that, the model, including data conversion and handling, interface, rate transition blocks, are built using standard SIMULINK blocks. Then, the host setup blocks from the Target Support toolbox are employed to the link between the Simulink model and real-world devices. Fig. 18 shows the proposed HIL architecture to present the relation

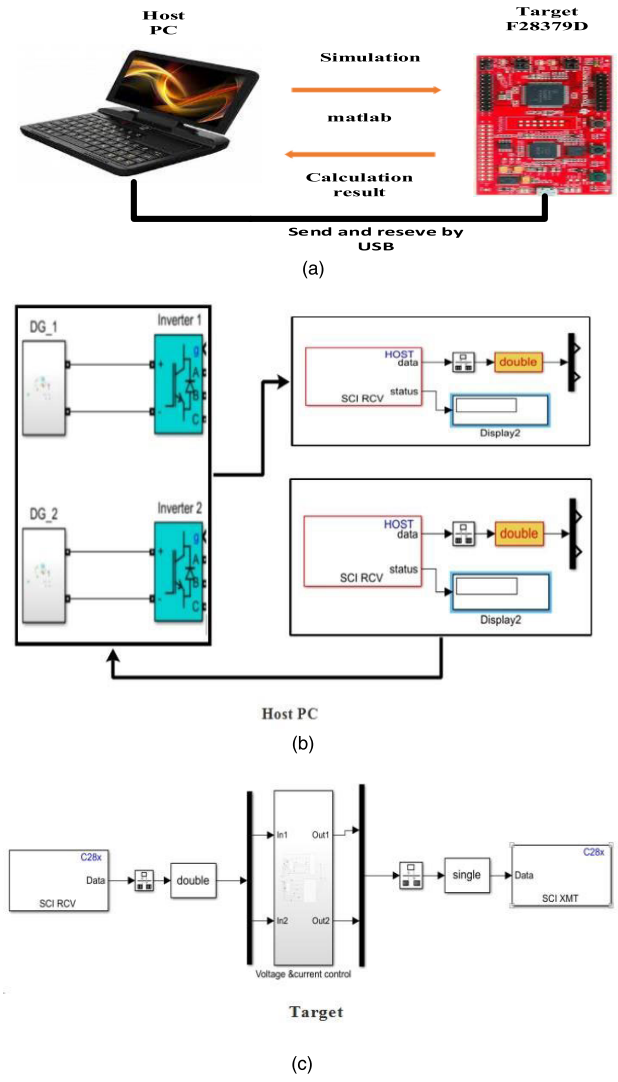

FIGURE 18. Block diagram of the proposed HIL using Launchpad TMS320F28379D a) general block of the system, b) the host system on PC and c) the target system on F28379D.

between the host PC and the target. On the host computer, both the PV and the inverters are constructed. The controllers are implemented on the LAUNCHXL-F28379D target for a typical HIL investigation.

On the other hand, all the remaining system components are simulated on the host PC. Each component can be implemented individually on the LAUNCHXL-F28379D due to the flexibility of the developed HIL-based testbed. The specifications of LAUNCHXL-F28379D are dual 200 MHz C28x cores, dual 200 MHz real-time control co-processor (CLA) and 1 MB flash and 204 KB RAM. In this section, more demonstrations on how to use the SIMULINK Support Package for Texas Instruments C2000 are introduced [30]. Moreover, the experimental validation of droop control using the new hybrid SSIA-PSO algorithm is performed. It is worth mentioning that the test bench is composed of three main parts: high-performance computer, LAUNCHXL-F28379D of Texas Instrument with USB connection and all required

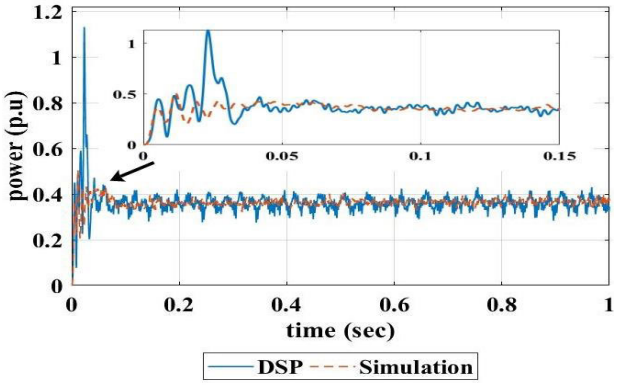

FIGURE 19. Active powers generated by DG_1 in DSP and simulation in IMFCL.

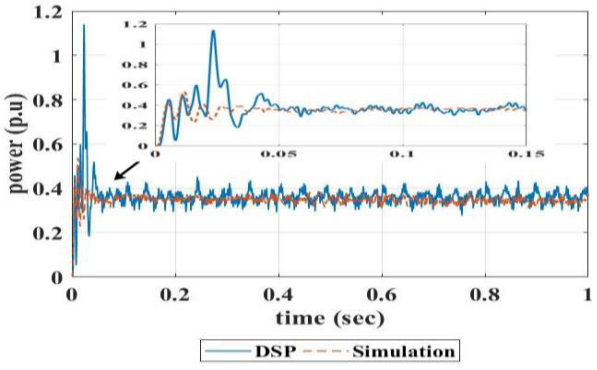

FIGURE 20. Active powers generated by DG_2 in DSP and simulation in IMFCLVS scenario.

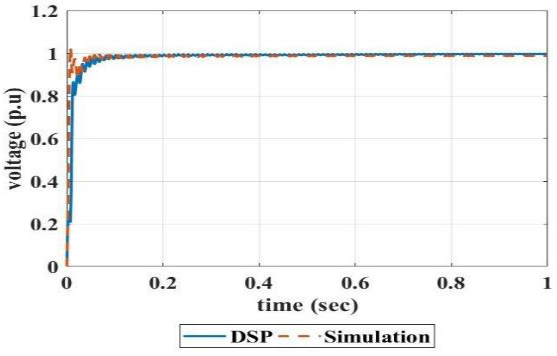

FIGURE 21. Voltage magnitude in DSP and simulation in IMFCLVS scenario.

software packages such as MATLAB/SIMULINK and Texas Instruments code composer. In the developed real-time HIL, the communication channel is established using USB to send and receive data from the host PC to the LAUNCHXL-F28379D and vice versa.

A. ISLANDING MODE WITH FIXED CYCLIC LOAD VARIATIONS SCENARIO (IMFCLVS)

The microgrid is worked in IMFCLVS with the same temperature 25 °C and solar irradiance 1000 W/m^2, in addition to the fixed load change pattern as 70 kW (0.7 p.u.).

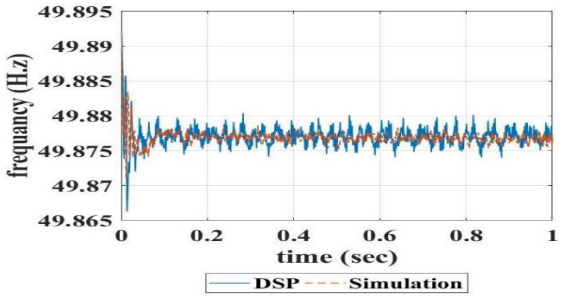

FIGURE 22. Inverter frequency in DSP and simulation in IMFCLVS scenario.

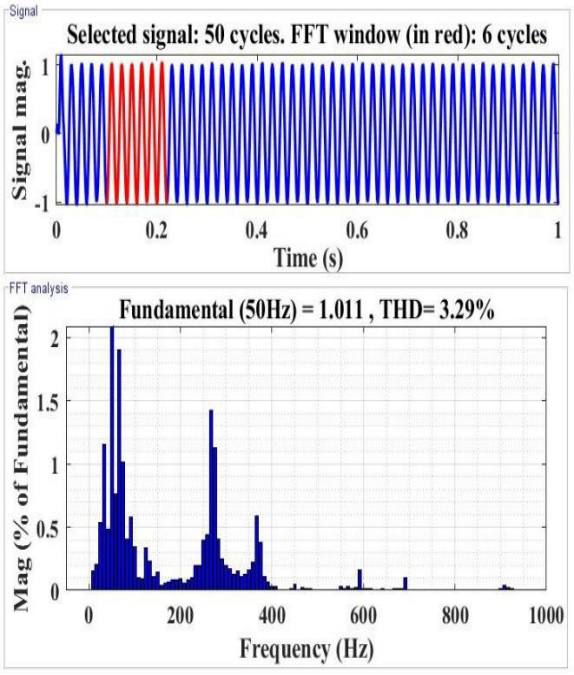

FIGURE 23. The FFT analysis in DSP of the proposed controller in DSP.

Fig. 19 shows that DG1 injects a similar amount of active power into the microgrid when using Digetal Signal Process (DSP) LAUNCHXL-F28379D compared to the MATLAB simulation but with tiny distortions in DSP results in the beginning. Fig. 20 displays the active power response for DG2 using the DSP LAUNCHXL-F28379D and MATLAB simulation. During this scenario (IMFCLVS), Fig. 21 and 22 demonstrate voltage and frequency responses, respectively. The inverter output waveform analysis is being evaluated by Fast Fourier Transform (FFT), as shown in Figures 23 and 24, respectively. The appropriate percentage of Total Harmonic Distortion (THD) in the electrical power supply must be less than 5 percent in compliance with IEEE Standard 1547–2003 [31]. As shown in figure 23, the THD obtained by employing the hybrid SSIA-PSO based controllers using DSP is 3.29 % compared to 3.25 % for the simulation, as illustrated in figure 24. It is worth stating that all the suggested controllers respected the THD permissible limits with a

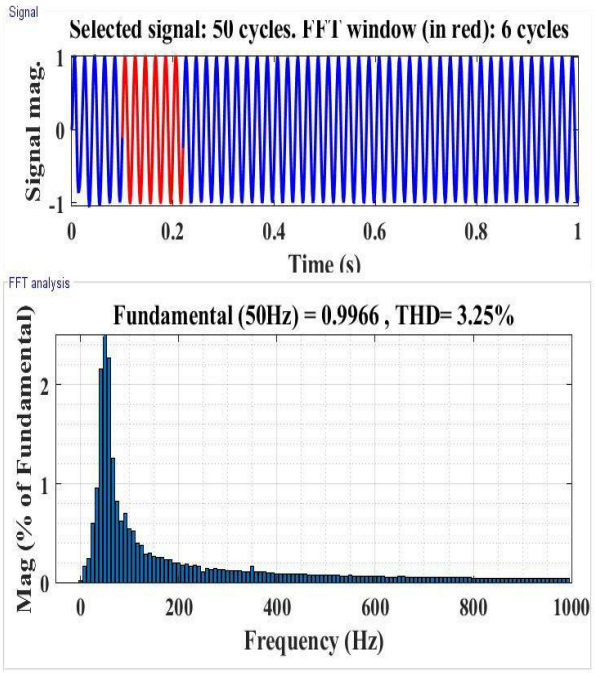

FIGURE 24. The FFT analysis in simulation of the proposed controller in simulation MATLAB.

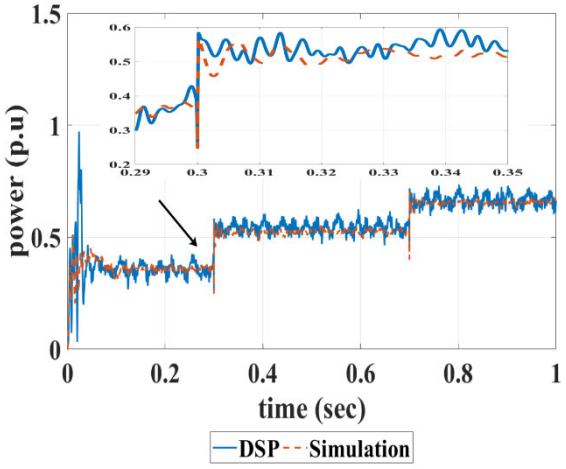

FIGURE 25. Active powers generated by DG_1 in DSP and simulation in IMCLVS scenario.

significant secure margin, which confirms the effectiveness of the suggested MG power architecture.

B. ISLANDING MODE WITH CYCLIC LOAD VARIATIONS SCENARIO (IMCLVS)

This scenario is just like the IMFCLVS scenario, but the differences are that the ramp loading is taken into account. The load value of 70 kW (0.7 p.u.) from 0-0.3 sec, then increased to 110 kW (1.1 p.u.) at 0.3 sec, then increased to 130 kW (1.3 p.u.) at 0.7 sec. Figures 25 and 26 illustrate the active power responses for both DG_1 and DG_2 using the DSP LAUNCHXL F28379D and MATLAB simulation.

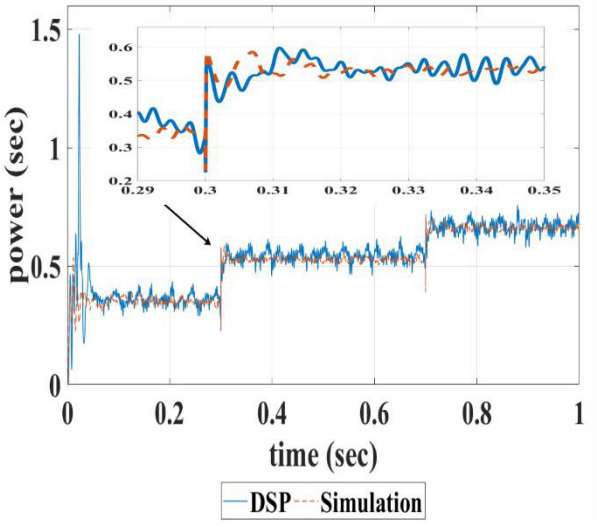

FIGURE 26. Active powers generated by DG_2 in DSP and simulation in IMCLVS scenario.

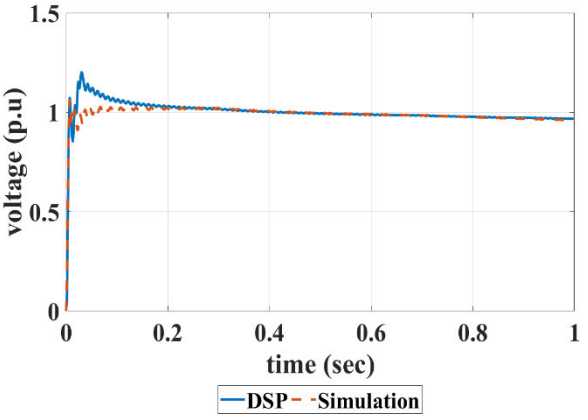

FIGURE 27. Voltage magnitude in DSP and simulation in IMCLVS scenario.

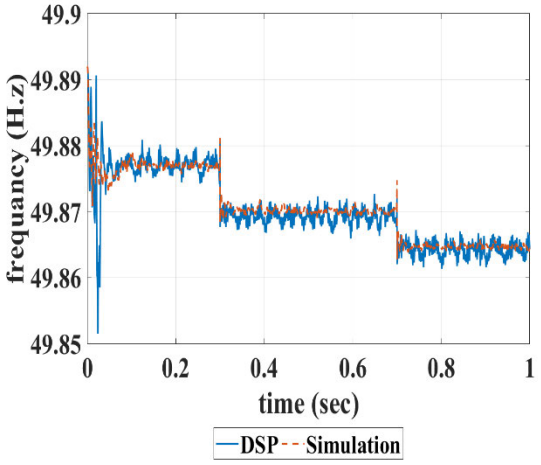

FIGURE 28. Inverter frequency in DSP and simulation in IMCLVS scenario.

Figures 27 and 28 indicate the voltage and frequency responses, respectively.

VII. CONCLUSION

This article proposes a new optimization algorithm, SSIA-PSO. The proposed SSIA-PSO is a hybrid technique merging both PSO and SSIA to benefit from the referential integrity property between their well-matured merits. The SSIA-PSO is applied on the twenty-three-benchmark problems to test its efficacy. The performance of SSIA-PSO is compared to seven metaheuristic algorithms. The analytical findings consistently show that SSIA-PSO is highly competitive and can be used for different engineering and other problems. After proving the efficiency of SSIA-PSO overall selected algorithms on the border, it was applied in the microgrid droop control field. There are two sources of a microgrid test system, and each source consists of a solar PV array, a battery station a supercapacitor.

The SSIA-PSO is used to find the gains of the PI controllers and the coefficients of the droop control scheme. The cost function consists of four types: IAE, ISE, ITAE, and ITSE. The best solution is attained when applying ITAE as an objective function. The quality of SSIA-PSO as an optimization tool was verified by the comparison with seven different types of optimizations techniques (SSIA, PSO, SCA, ALO, DA, ABC and GWO-PSO) applied to the microgrid scheme. The attained gains of PI controllers and the droop control coefficients K_{p1}, K_{i1}, K_{p2}, K_{i2}, K_{p3}, K_{i3}, K_{p4}, K_{i4}, nq, m_p are applied in the system during two scenarios. The suggested scenarios consider slow and fast changes as well as sudden and ramp variations in both renewable energy resources and loads. The simulation results revealed that the power-sharing amongst the paralleled DGs had been achieved and thanks to SSIA-PSO based droop control strategy. The frequency deviation is within the permissible range and the DGs are rapidly following changes in load with a good dynamic response. Also, this article introduces a real-time testbed to test the suggested control in real-time by using LAUNCHXL-F28379D. The proposed scenarios consider fixed as well as slow and rapid shifts in load variations are conducted to validate the efficacy of the experimental setup. The experimental results are very close to the simulation results with tiny distortions at the startup of the DSP. In the case of DSP, the THD is 3.29% compared to 3.25% in the simulation case. Although the advantages of the proposed method, it needs more elaborations on large scale systems with many parameters to be optimized under different uncertainties. In this context, the authors propose to employ the suggested approach for solving different multi-objective engineering problems.

REFERENCES

[1] A. Khaledian, A. Ahmadian, and M. Aliakbar-Golkar, "Optimal droop gains assignment for real-time energy management in an islanding microgrid: A two-layer techno-economic approach," *IET Gener., Transmiss. Distrib.*, vol. 11, no. 9, pp. 2292–2304, Jun. 2017, doi: 10.1049/iet-gtd.2016.1718.

[2] M. Kohansal, G. B. Gharehpetian, and M. Abedi, "An optimization to improve voltage response of VSI in islanded microgrid considering reactive power sharing," in *Proc. 2nd Iranian Conf. Renew. Energy Distrib. Gener. (ICREDG)*, Mar. 2012, pp. 127–131, doi: 10.1109/ICREDG.2012.6190447.

[3] Z. Li, Z. Cheng, J. Liang, J. Si, L. Dong, and S. Li, "Distributed event-triggered secondary control for economic dispatch and frequency restoration control of droop-controlled AC microgrids," *IEEE Trans. Sustain. Energy*, vol. 11, no. 3, pp. 1938–1950, Jul. 2020, doi: 10.1109/TSTE.2019.2946740.

[4] D. K. Dheer, Y. Gupta, and S. Member, "A self adjusting droop control strategy to improve reactive power sharing in islanded microgrid," *IEEE Trans. Sustain. Energy*, vol. 11, no. 3, pp. 1624–1635, Jul. 2020, doi: 10.1109/TSTE.2019.2933144.

[5] D. Yang, Z. Xu, W. Li, and F. Bu, "Droop control strategy of the AC/DC hybrid micro-grid based on quasi-PR control," *J. Eng.*, vol. 2017, no. 14, pp. 2634–2642, Jan. 2017, doi: 10.1049/joe.2017.0840.

[6] P. Yang, M. Yu, Q. Wu, P. Wang, Y. Xia, and W. Wei, "Decentralized economic operation control for hybrid AC/DC microgrid," *IEEE Trans. Sustain. Energy*, vol. 11, no. 3, pp. 1898–1910, Jul. 2020, doi: 10.1109/TSTE.2019.2946227.

[7] S. Mirjalili and S. Z. M. Hashim, "A new hybrid PSOGSA algorithm for function optimization," in *Proc. Int. Conf. Comput. Inf. Appl.*, no. 1, Dec. 2010, pp. 374–377, doi: 10.1109/ICCIA.2010.6141614.

[8] S. Mirjalili, A. H. Gandomi, S. Z. Mirjalili, S. Saremi, H. Faris, and S. M. Mirjalili, "Salp swarm algorithm: A bio-inspired optimizer for engineering design problems," *Adv. Eng. Softw.*, vol. 114, pp. 163–191, Dec. 2017, doi: 10.1016/j.advengsoft.2017.07.002.

[9] N. Aouchiche, M. S. Aitcheikh, M. Becherif, and M. A. Ebrahim, "AI-based global MPPT for partial shaded grid connected PV plant via MFO approach," *Sol. Energy*, vol. 171, pp. 593–603, Sep. 2018, doi: 10.1016/j.solener.2018.06.109.

[10] K. Dasgupta, P. K. Roy, and V. Mukherjee, "Power flow based hydro-thermal-wind scheduling of hybrid power system using sine cosine algorithm," *Electr. Power Syst. Res.*, vol. 178, Jan. 2020, Art. no. 106018, doi: 10.1016/j.epsr.2019.106018.

[11] M. Maher, M. A. Ebrahim, E. A. Mohamed, and A. Mohamed, "Ant-lion inspired algorithm based optimal design of electric distribution networks," in *Proc. 19th Int. Middle East Power Syst. Conf. (MEPCON)*, Dec. 2017, pp. 613–618, doi: 10.1109/MEPCON.2017.8301244.

[12] S. Mirjalili, S. M. Mirjalili, and A. Lewis, "Grey wolf optimizer," *Adv. Eng. Softw.*, vol. 69, pp. 46–61, Mar. 2014, doi: 10.1016/j.advengsoft.2013.12.007.

[13] L.-L. Li, X. Zhao, M.-L. Tseng, and R. R. Tan, "Short-term wind power forecasting based on support vector machine with improved dragonfly algorithm," *J. Cleaner Prod.*, vol. 242, Jan. 2020, Art. no. 118447, doi: 10.1016/j.jclepro.2019.118447.

[14] S. Khunkitti, A. Siritaratiwat, S. Premrudeepreechacharn, R. Chatthaworn, and N. Watson, "A hybrid DA-PSO optimization algorithm for multiobjective optimal power flow problems," *Energies*, vol. 11, no. 9, p. 2270, Aug. 2018, doi: 10.3390/en11092270.

[15] S. Kaur and R. Mahajan, "Hybrid meta-heuristic optimization based energy efficient protocol for wireless sensor networks," *Egyptian Informat. J.*, vol. 19, no. 3, pp. 145–150, Nov. 2018, doi: 10.1016/j.eij.2018.01.002.

[16] T. A. Jumani, M. W. Mustafa, M. M. Rasid, N. H. Mirjat, Z. H. Leghari, and M. S. Saeed, "Optimal voltage and frequency control of an islanded microgrid using grasshopper optimization algorithm," *Energies*, vol. 11, no. 11, p. 3191, Nov. 2018, doi: 10.3390/en11113191.

[17] F. A. Şenel, F. Gökçe, A. S. Yüksel, and T. Yiğit, "A novel hybrid PSO–GWO algorithm for optimization problems," *Eng. Comput.*, vol. 35, no. 4, pp. 1359–1373, 2019, doi: 10.1007/s00366-018-0668-5.

[18] M. A. Kamarposhti, "Optimal control of islanded micro grid using particle swarm optimization algorithm," *Int. J. Ind. Electron., Control Optim.*, vol. 1, no. 1, pp. 53–60, 2018.

[19] G. Ellis, "Model development and verification," *Control Syst. Des. Guid.*, pp. 261–282, 2012, doi: 10.1016/b978-0-12-385920-4.00013-8.

[20] A. Kurt, M. Vernier, S. Biddlestone, K. Redmill, and Ü. Özgüner, "Testing of intelligent vehicles using virtual environments and staged scenarios," in *Proc. Adv. Intell. Vehicles*, 2013, pp. 45–64, doi: 10.1016/B978-0-12-397199-9.00002-1.

[21] J. Aravena, D. Carrasco, M. Diaz, M. Uriarte, F. Rojas, R. Cardenas, and J. C. Travieso, "Design and implementation of a low-cost real-time control platform for power electronics applications," *Energies*, vol. 13, no. 6, pp. 1–15, 2020, doi: 10.3390/en13061527.

[22] M. Settles, *An Introduction to Particle Swarm Optimization*. London, U.K.: Springer, 2005, pp. 1–8, doi: 10.1038/nmat3280.

[23] S. A. Pourmousavi, M. H. Nehrir, C. M. Colson, and C. Wang, "Real-time energy management of a stand-alone hybrid wind-microturbine energy system using particle swarm optimization," *IEEE Trans. Sustain. Energy*, vol. 1, no. 3, pp. 193–201, Oct. 2010.
[24] D. P. Rini, "Particle swarm optimization: Technique, system and challenges," *Int. J. Comput. Appl.*, vol. 14, no. 1, pp. 19–27, 2011.
[25] M. H. Qais, H. M. Hasanien, and S. Alghuwainem, "Enhanced salp swarm algorithm: Application to variable speed wind generators," *Eng. Appl. Artif. Intell.*, vol. 80, pp. 82–96, Apr. 2019, doi: 10.1016/j.engappai.2019.01.011.
[26] B. Yang, L. Zhong, X. Zhang, H. Shu, T. Yu, H. Li, L. Jiang, and L. Sun, "Novel bio-inspired memetic salp swarm algorithm and application to MPPT for PV systems considering partial shading condition," *J. Cleaner Prod.*, vol. 215, pp. 1203–1222, Apr. 2019, doi: 10.1016/j.jclepro.2019.01.150.
[27] K. Yu, Q. Ai, S. Wang, J. Ni, and T. Lv, "Analysis and optimization of droop controller for microgrid system based on small-signal dynamic model," *IEEE Trans. Smart Grid*, vol. 7, no. 2, pp. 695–705, Mar. 2016, doi: 10.1109/TSG.2015.2501316.
[28] K. M. Hussain, R. A. R. Zepherin, M. S. Kumar, and S. M. G. Kumar, "Comparison of PID controller tuning methods with genetic algorithm for FOPTD system," *J. Eng. Res. Appl.*, vol. 4, no. 2, pp. 308–314, 2014.
[29] *Hardware in the Loop From the MATLAB / Simulink Environment*, A. Corporation, Sep. 2013. pp. 1–9. [Online]. Available: https://www.altera.com/content/dam/altera-www/global/en_US/pdfs/literature/wp/wp-01208-hardware-in-the-loop.pdf
[30] R. Duma, P. Dobra, M. Abrudean, and M. Dobra, "Rapid prototyping of control systems using embedded target for TI C2000 DSP," in *Proc. Medit. Conf. Control Autom.*, Jun. 2007, pp. 1–5, doi: 10.1109/MED.2007.4433860.
[31] W. S. Read, "IEEE standards," *IEEE Power Eng. Rev.*, vol. 15, no. 1, pp. 6–7, Jan. 1995, doi: 10.1109/MPER.1995.350411.

M. A. EBRAHIM (Senior Member, IEEE) received the B.Sc., M.Sc., and Ph.D. degrees in electrical engineering from the Faculty of Engineering at Shoubra, Benha University, Cairo, Egypt, in 2004, 2009, and 2013, respectively.

He took up Demonstrator's rank, an Assistant Lecturer, and a Lecturer with Benha University in 2005, 2009, and 2013, respectively, and has been an Associate Professor, since 2018. His research interests include analyzing, designing, and controlling electric power systems, new, and renewable energy applications. He has been published 73 scientific articles and five book chapters in international book series. He did several Postdoctoral Research Missions with the Federation of Research of Fuel Cells and the University of Technology of Belfort-Montbéliard, Belfort, France. He is the PI and the Coordinator of different Egyptian–French projects. He is a Reviewer for several the IEEE TRANSACTIONS, IET, and different Elsevier journals.

REHAM MOHAMED ABDEL FATTAH received the B.Sc. and M.Sc. degrees in electrical engineering from the Faculty of Helwan University, Cairo, Egypt, in 2004 and 2011, respectively. Her research interests include renewable energy, microgrid, and optimization technique.

EBTISAM MOSTAFA MOHAMED SAIED received the B.Sc., M.Sc., and Ph.D. degrees in electrical engineering from the Faculty of Engineering Cairo University, Cairo, Egypt, in 1982, 1986, and 1992, respectively. Since 2003, she became a Professor of electrical engineering from the Faculty of Engineering at Shoubra, Benha University, Cairo. Her research interests include electrical power engineering, power systems, and renewable energy applications.

SAMIR MOHAMED ABDEL MAKSOUD received the B.Sc., M.Sc., and Ph.D. degrees in electrical engineering from the Faculty of Engineering at Shoubra, Zagazig University (Benha Branch), Cairo, Egypt, in 1983, 1992, and 2003 respectively. His research interests include analysis, electrical power engineering, power systems, and economic load dispatching voltage instability.

HISHAM EL KHASHAB was born in Cairo, Egypt, in 1952. He received the B.Sc. and M.Sc. degrees from Cairo University, Egypt, in 1973 and 1977, respectively, and the Ph.D. degree in electrical engineering from the National Institute of Polytechnics of Grenoble, France, in May 1982.

Since 1996, he has been a Professor of the Power Electronics and Energy Conversion Department, Electronics Research Institute, National Research Centre of Cairo. His current research interests include power electronics, electrical machines and drives, and renewable energy. He has supervised several M.Sc. and Ph.D. Theses. In 2004, he was a Visiting Professor with the Yanbu Industrial College for ten years. He has participated in establishing a renewable energy center for education and society awareness. His main research interests include renewable energy systems, micro-grid control, and power electronics.